J. Astron. Space Sci. 12(2), 157–167 (1995)

MODEL DUST ENVELOPES FOR ASYMPTOTIC GIANT BRANCH STARS. I. OH/IR STARS

Kyung-Won Suh
Department of Astronomy and Space Science, Chungbuk National University
e-mail: kwsuh@astro.chungbuk.ac.kr

(Received September 28, 1995; Accepted October 20, 1995)

ABSTRACT

OH/IR stars are the most massive and youngest subclasss in asymptotic giant branch stars which pass through sporadic superwind phases. We have modeled the dust envelopes around OH/IR stars with close attention to the evolution of the structure of the dust shells. We use various dust density distributions to take account the effect of the superwind due to the helium shell flash by adding a density increased region. Depending on the position and quality of the density increased region, the model results are different from the results with conventional density distribution. The new results fit the observations of some OH/IR stars better. Especially, the OH/IR stars with excessive 30-100 μm emission can be better explained by the new results. The IR two-color diagrams comparing the results of the superwind models and IRAS observation of 95 OH/IR stars have been made. The new results can explain much wider regions on the IR two-color diagrams.

1. INTRODUCTION

As asymptotic giant branch (AGB) stars evolve to planetary nebulae, thermal pulses due to sporadic helium shell flashs have been considered to be one of the major cause of increasing mass loss. Planetary nebulae often show two, and sometimes three, shell like structures around them (*e.g.*, Balick *et al.* 1992). These may be due to abrupt changes in the mass loss rate back when the star was a dusty AGB stars. Conventional wisdom indicates that these shells are the result of thermal pulsing (helium shell flashes) during the past history of the star.

The basic idea is that the dormant helium shell around the carbon and oxygen degenerate core of an AGB star suddenly starts fusing helium into carbon for a few hundred years. The presence of distinct shells of material around planetary nebulae suggests these thermal pulse episodes strongly modulate the mass-loss rate from the star. In other words, while

a thermal pulse is taking place, the mass-loss rate from the AGB star increases by about a factor of 10 for the duration of the pulse. The stellar wind becomes stronger and mass loss rate gets bigger during this superwind phase. And then goes back to initial state. We expect about 10 - 100 superwind events during AGB stage depending on the mass and chemical composion of the star.

In this paper, we investigate the influence of the superwind on the spectral energy distribution of OH/IR stars. We modify the dust density distribution by adding a density increased region. We try to simulate the influence of the superwind using above method and to compare in detail the new results with previous model results and the observed spectral energy distribution (SED) of the OH/IR stars.

2. PROCEDURES OF RADIATIVE TRANSFER MODEL CALCULATIONS

Dust grains in the outer shells of OH/IR stars absorb and scatter the stellar radiation and reemit it at longer wavelengths. For given characteristics of the central star and the dust shell around it, we may find the emergent spectra by solving the radiative transport processes and compare the results with observations. We may check whether our modeling is accurate or not and find ways to improve our input parameters. We have used Leung's radiative transfer code (Egan *et al.* 1988). In the present calculations, a radial grid of 125 points and a frequency grid of 70 wavelengths were used. The parameters for central hot source which is assumed to be a black body are the temperature and the luminosity. And the parameters for dust envelope are dust opacity at different wavelengths, the optical depth, and the dust density distribution.

The dust condensation temperature (T_c) is assumed to be 1000 K and the dust condensation radius (R_c) is obtained after a few trials. The outer radius of the dust shell is always taken to be 1000 R_c. The radii of spherical dust grains have been assumed to be 0.1 μm uniformly. Finally, the dust optical depth (τ) at 9.7 μm is obtained to fit the observations of each object.

For the central hot source, the luminosity is taken to be $1 \times 10^4 L_\odot$ and the black body temperature of 2000 K is assumed for all OH/IR stars modeled in this work. The change of the luminosity does not affect the shape of the output spectra, it only affects the overall energy output throughout wide wavelength ranges. But the change of the central blackbody temperature does affect the output spectra. Even the minor temperature changes between 2000 K and 3000 K do make differences. For all the OH/IR stars that will be mentioned here, the temperature 2000 K fits best.

2.1 Dust Opacity

The optical constants (n, k) are parts of index of refraction ($m = n + i\,k$). We have

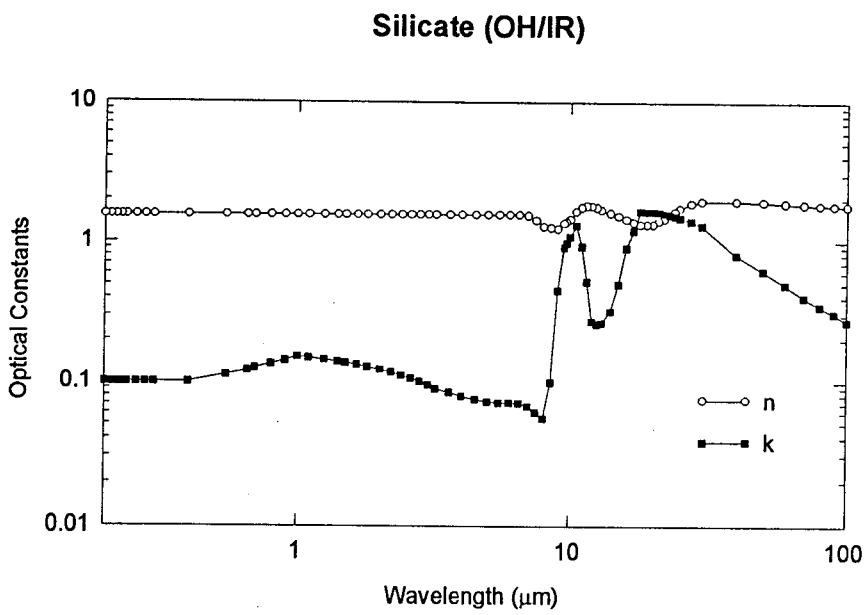

Figure 1. Optical Constants.

obtained a set of optical constants adapting both experimental data and model fitting with observations. In the limit of very small grains, the spectral profile of the absorption and extinction efficiencies are independent of grain size but simply related to the imaginary index of refraction, k (Prégourié & Papoular 1985). So we have used laboratory values of n for a typical candidate material Mg_2SiO_4. Day (1979)'s values for $\lambda = 8 - 30\mu$m and Day (1981)'s values for $\lambda = 30 - 100\mu$m are used for n. And k is deduced from both experimental above data and model fitting using conventional dust density distribution for some well observed OH/IR stars. For shorter wavelengths, we adopted similar values to those of Draine & Lee (1984) smoothly joined to our values at longer wavelengths.

Figure 1 shows the optical constants versus wavelength. And figure 2 shows the absorption and scattering efficiency factors versus wavelength for spherical dust grain with radius 0.1 μm. This opacity pattern closely resembles to the opacity pattern used by many authors for modeling OH/IR stars with conventional density distribution (*e.g.*, Bedijin 1987, Volk & Kwok 1988, Groenewegen 1994).

2.2 Dust Density Distribution

Radiative transfer models for AGB stars are developed by a number of authors with various assumptions on input parameters and degrees of sophistication (*e.g.*, Jones & Merrill

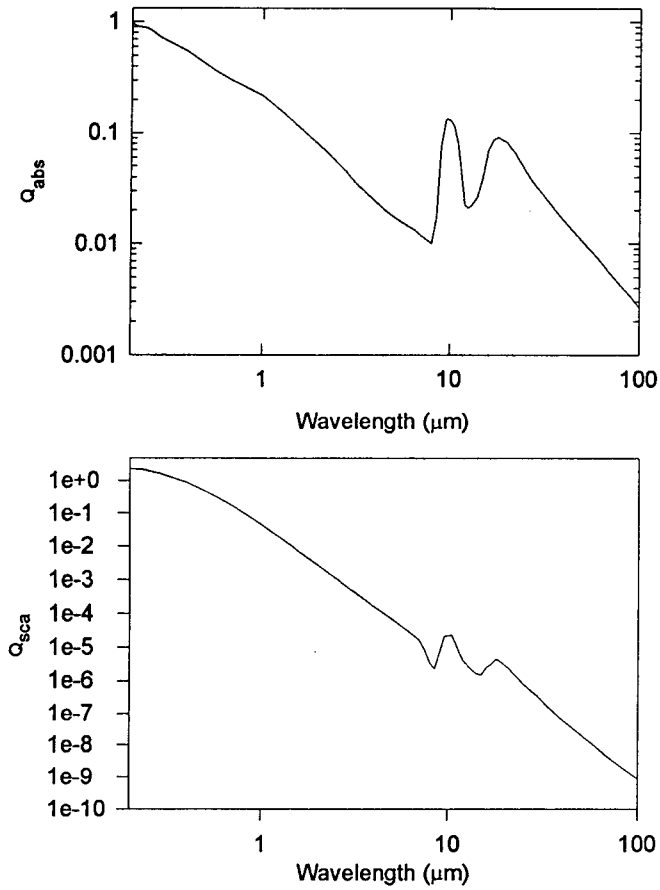

Figure 2. Absorption and Scattering efficiency factors.

1976, Volk & Kwok 1988, Suh 1991) assuming a smoothly distributed spherical symmetric dust shell. The dust density distribution was assumed to be inversely proportional to the square of the distance. But if we take the effects of the superwinds into account, the dust density distribution should be different from the smooth distribution.

We expect one thermal pulse per each $10^4 - 10^5$ years which endure for about 100-1000 years. The dust condensation radius from the center of the central star (R_c) is about 0.1×10^{-3} pc for typical OH/IR stars. The expansion velocity is about 10 - 20 km/sec. A change in the dust density distribution will affect the outgoing spectra. The effect will be different depending on the location of the change, and the change up to 1000 R_c will do affect the outgoing energy spectra. The travel time for 1000 R_c is about 6000 years which

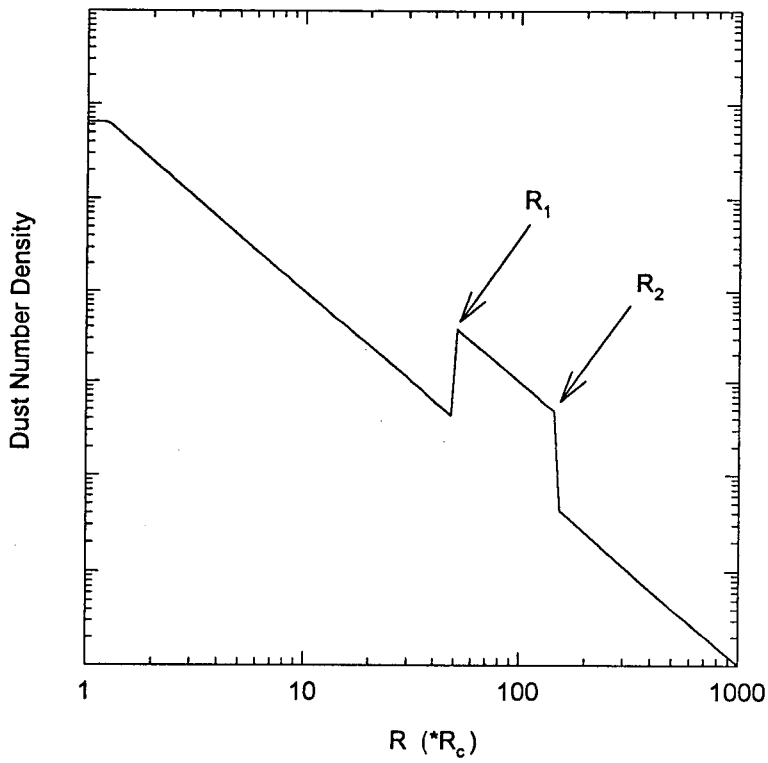

Figure 3. Dust Density Distribution.

is smaller than thermal pulse period. So there should be only one discontinuity. We may expect that a significant portion of AGB stars have that discontinuity in their dust shells. And we may expect that about a half of the AGB stars have the discontinuity in their dust shells at various radii. The shape of discontinuity in the dust density distribution would be like figure 3. The density suddenly increases at R_2 then goes back to initial state at R_1.

Let's see the effect of density increase with different degrees. Figure 4 shows the results with the same optical depth (τ = 15) conventional model and two super wind models with R_1=100 R_c and R_2=200 R_c; one with the density incresed by 10 times and other with density increased by 50 times.

Figure 5 shows the results with the same with the same optical depth (τ = 15) and the density increase of 10 but with different locations of the discontinuity. As the location get farther from the central star, the effect gets smaller. We see the qualitative difference from figure 4 and figure 5. Depending on the position and quality of the discontinuity, the results are very different from the results with conventional density distribution.

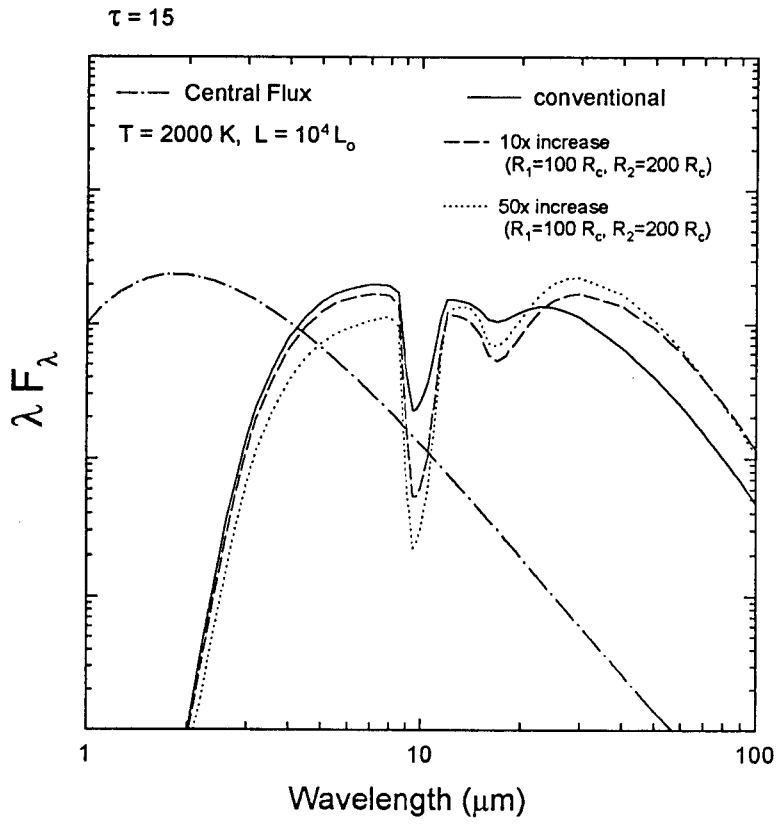

Figure 4. Model Results with different degree of density increase.

3. SPECTRAL ENERGY DISTRIBUTION COMPARISON

The SEDs of many OH/IR stars are from various sources. Especially the third catalog of infrared observations (Gezari *et al.* 1993) has been very useful. The observational data are from many references for last 20 years of infrared observations of OH/IR stars. We have obtained the results of model calculations with various possible stellar and dust envelope parameters. The results are compared with observations and more reliable input parameters are obtained. The data are mostly in infrared magnitudes or Jansky unit. They are converted to an absolute flux unit (λF_λ; Watts/cm^2) by zero magnitude calibration processes using the instrument's characters mentioned in each paper (see e.g., Gehrz *et al.* 1987). Our new model can explain some of the odd SEDs fairly well.

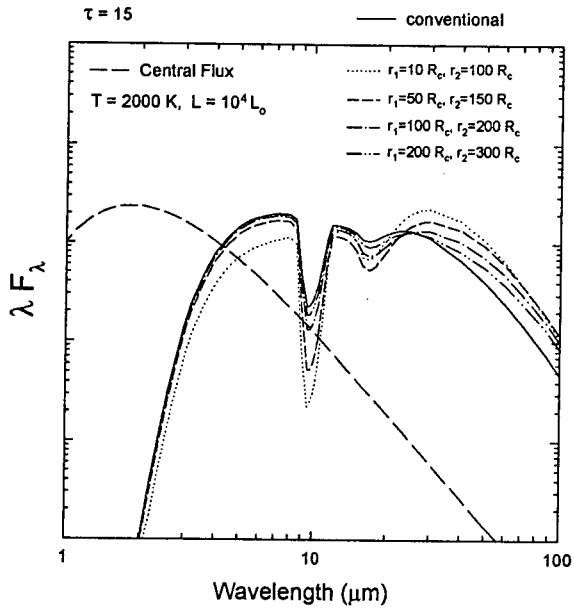

Figure 5. Model Results with different location of discontinuity (density increased by 10 times).

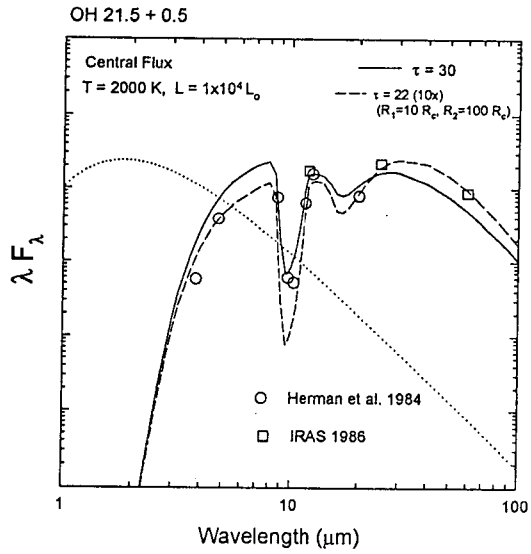

Figure 6. Model Results compared with Observations for OH 21.5 + 0.5.

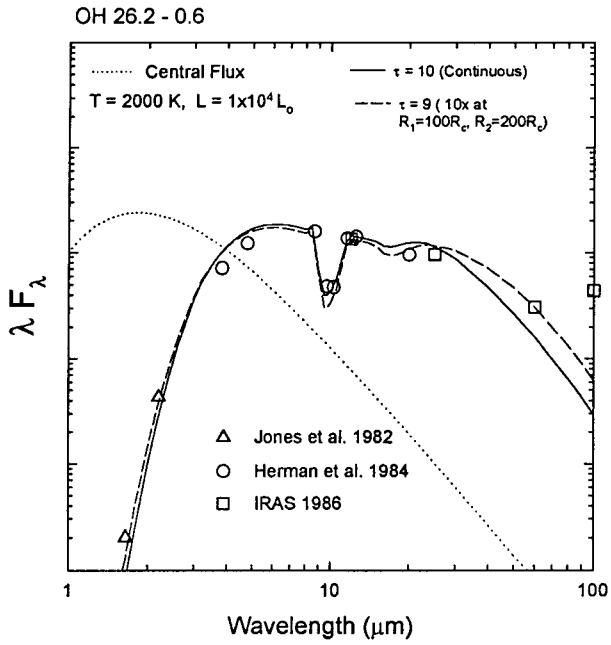

Figure 7. Model Results compared with Observations for OH 26.2 - 0.6.

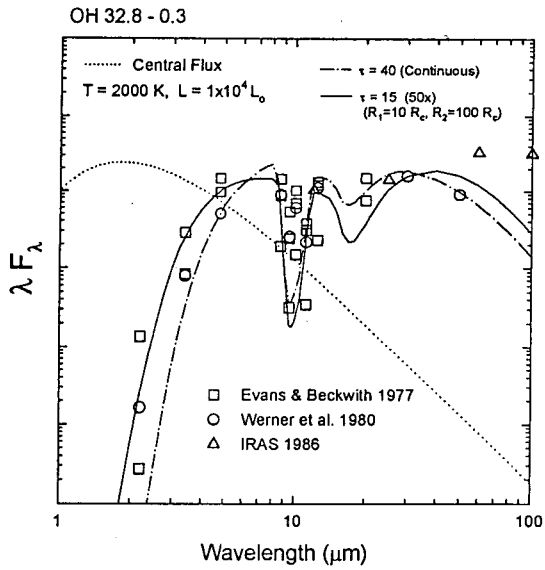

Figure 8. Model Results compared with Observations for OH 32.8 - 0.3.

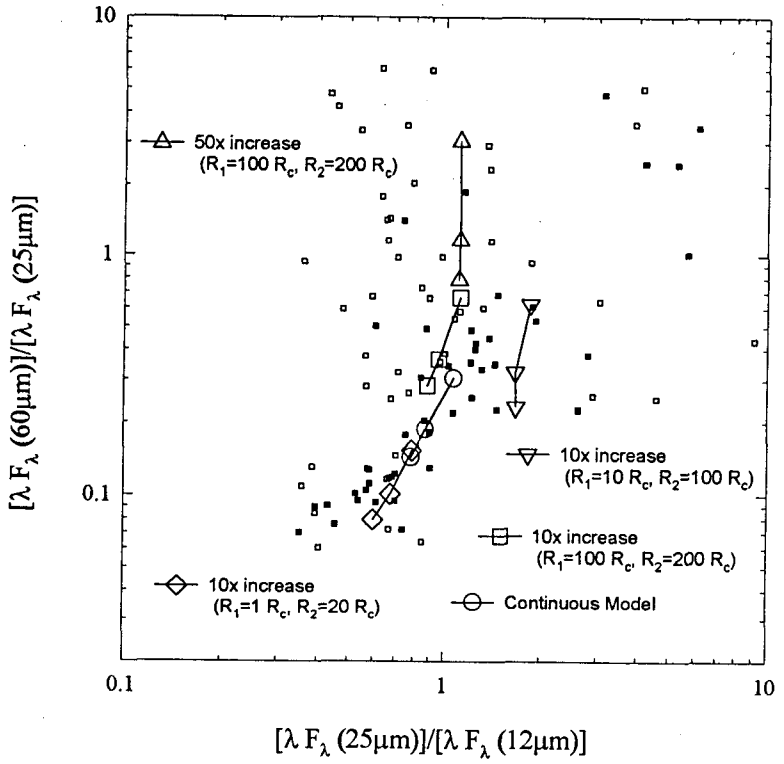

Figure 9. Model Results compared with IRAS Observations on IR 2-color Diagram.

We have compared the results with the observed SEDs of the following OH/IR stars; OH 21.5 + 0.5, OH 26.2 - 0.6, and OH 32.8 - 0.3. Figure 6 shows the results of the model calculations (lines) superimposed on observational data (symbols) for OH 21.5 + 0.5. Figure 7 and 8 show the results for OH 26.2 - 0.6, OH 32.8 - 0.3 respectively. The new results fit the observations of these OH/IR stars better. Especially, the OH/IR stars with excessive 30-100 μm emission can be better explained by new results. This is more clear when we consider IRAS 2-Color diagrams in the next section.

4. COMPARISON ON IRAS 2-COLOR DIAGRAMS

IRAS 4-color photometric data (IRAS 1986) are available for 105 OH/IR stars. On figure 9, small squares represent observational data (empty squares represent the data with poor quality, *i.e.* they are upper limit values for 60, 100 μm data) while lines and big symbols represent the model calculation results ($\tau_{\lambda=9.7\mu m}$ = 10, 15, 30). Continuous (conventional) models do not go into upper right corner while other models with discontinuity

do. Depending on the position and quality of the density increase, the model results are very different. The superwind model results can expalin the various positions on the IR 2-color diagram of OH/IR stars.

5. DISCUSSION

The superwind model results fit the observations of some OH/IR stars better. Especially, the OH/IR stars with excessive 30-100 μm emission can be better explained by the new results. The conventional models with continuous density distribution ($\rho \propto r^{-2}$) can not explain the SEDs of those OH/IR stars even with various changes of other parameters. But it is hard to distinguish which model explain better for following OH/IR stars; OH 20.7 + 0.1, OH 21.5 + 0.5, and OH 26.5 + 0.6 (Suh 1995). The effects of the superwinds on SEDs in IR could be not prominent depending on the position of the density increase. So even if a star has a density increase in their shell, the observed SED could be almost the same as that of a star without density increase.

The effect of the superwind would be more prominent in proto planetary nebula stage. The optical image of the mutiple shells may unveil the past history of the superwinds much better than dust thick AGB stars. But the image is made much later than the time of the production of the distinguished shells of planetary nebulae.

ACKNOWLEDGMENTS: This paper was supported by the Basic Science Institute Program, Ministry of Education, 1994, Project No. BSRI-94-5413.

REFERENCES

Balick, B., Gonzalez, G., Frank, A. & Jacoby, G. 1992, ApJ, 392, 582
Bedijin, P. J. 1987, A&A, 186, 136
Day, K. L. 1979, ApJ, 234, 158
Day, K. L. 1981, ApJ, 246, 110
Draine, B. T. & Lee, H. M. 1984, ApJ, 285, 89
Egan, M. P., Leung, C. M. & Spagna, G. F., Jr. 1988, Computer Phy. Comm., 48, 271
Evans II, N. J. & Beckwith, C. 1977, ApJ, 217, 729
Gehrz, R. D., Grasdalen, G. L. & Hackwell, J. A. 1987, in The Encyclopedia of Physical Science & Technology, 2, 53
Gezari, D. Y., Schmitz, M., Pitts, P. S. & Mead, J. M. 1993, Catalog of Infrared Observations, Third Edition, NASA Reference Publication 1294
Groenewegen, M. A. T. 1994, A&A, 290, 544

Herman, J., Isaacman, R., Sargent, A. & Habing, H. J. 1984, A&A, 139, 171
Iben, I. 1981, ApJ, 246, 278
IRAS catalogues and atlases 1986, Point Source Catalogue, US Government Publication Office
Jones, T. J., Hyland, A. R., Caswell, J. L. & Gatley, I. 1982, ApJ, 253, 208
Jones, T. W. & Merrill, K. M. 1976, ApJ, 209, 509
Prégourié, B. & Papoular, R. 1985, A&A, 142, 451
Suh, K. W. 1991, Ap&SS, 181, 237
Suh, K. W. 1995, in preparation
Volk, K. & Kwok, S. 1988, ApJ, 331, 435
Werner, M. W., Beckwith, S., Gatley, I., Sellgren, K., Berriman, G. & Whiting, D. L. 1980, ApJ, 239, 540